CZECH TECHNICAL UNIVERSITY IN PRAGUE

Faculty of Nuclear Sciences and Physical Engineering

Department of Physics

Research Project

Non-identical kaon femtoscopy at STAR experiment

Jindřich Lidrych

Supervisor: RNDr. Petr Chaloupka, Ph.D.

Prague, 2015

ČESKÉ VYSOKÉ UČENÍ TECHNICKÉ
V PRAZE
Fakulta jaderná a fyzikálně inženýrská
Katedra fyziky

Výzkumný úkol

Femtoskopie neidentických kaonů na experimentu STAR

Jindřich Lidrych

Vedoucí práce: RNDr. Petr Chaloupka, Ph.D.

Praha, 2015

ČESKÉ VYSOKÉ UČENÍ TECHNICKÉ V PRAZE
FAKULTA JADERNÁ A FYZIKÁLNĚ INŽENÝRSKÁ
PRAHA 1 - STARÉ MĚSTO, BŘEHOVÁ 7 - PSČ 115 19

Katedra: fyziky **Akademický rok:** 2014/2015

VÝZKUMNÝ ÚKOL

Posluchač: Bc. Jindřich Lidrych

Obor: Experimentální jaderná a částicová fyzika

Vedoucí úkolu: RNDr. Petr Chaloupka, Ph.D., FJFI ČVUT

Název úkolu (česky/anglicky):

Femtoskopie neidentických kaonů na experimentu STAR / Non-identical kaon femtoscopy at STAR experiment

Pokyny pro vypracování:

V rámci své práce se student blíže seznámí s femtoskopickými korelacemi neidentických částic. Student se bude také účastnit analýzy dat experimentu STAR ze srážek jader zlata při těžišťové energii $\sqrt{s_{NN}}$ = 200 GeV. Hlavním cílem bude konstrukce a analýza korelační funkce neidentických kaonů. K tomu se bude student muset naučit využívat data z detektorů nutných pro analýzu – časová projekční komora a detektor doby letu.

Práce bude vypracována v anglickém jazyce.

Součástí zadání výzkumného úkolu je jeho uložení na webové stránky katedry fyziky.

Literatura:

[1] K.Yagi et al., Quark-Gluon Plasma, Cambridge University Press 2005.
[2] M. A. Lisa et al, Ann.Rev.Nucl.Part.Sci. 55 (2005) 357-402.
[3] M. A. Lisa and S. Pratt, arXiv:0811.1352[nucl-ex]
[4] R. Lednicky et al., Phys.Part.Nucl. 40 (2009) 307-352
[5] R. Lednicky et al., Prog.Theor.Phys.Suppl. 193 (2012) 335-339
[6] S.V. Afanasiev et al., Physics Letters B 557 (2003) 157–166

Datum zadání: 16.10.2014 .....

Datum odevzdání: 26.06.2015 ***Vedoucí katedry***

Prohlášení:

Prohlašuji, že jsem svůj výzkumný úkol vypracoval samostatně a použil jsem pouze podklady (literaturu, software, atd.) uvedené v přiloženém seznamu.

Nemám závažný duvod proti užití tohoto školního díla ve smyslu 60 Zákona .121/2000 Sb., o právu autorském, o právech souvisejících s právem autorským a o změně některých zákonu (autorský zákon).

V Praze dne 10. září 2015

Jindřich Lidrych

Title:
Non-identical kaon femtoscopy at STAR experiment

Author: Jindřich Lidrych

Specialization: Experimental nuclear and particle physics

Sort of project: Research project

Supervisor: RNDr. Petr Chaloupka, Ph.D.

Abstract:

High energy heavy ion collisions provide means to study properties of nuclear matter under the extreme conditions. It is expected that a new state of matter called quark-qluon plasma is created during these collisions. Femtoscopic measurements of two-particle correlations at small relative momenta reveal information about the space-time characteristics of the system at the moment of particle emission. The correlations result from quantum statistics, final-state Coulomb interactions, and the strong final-state interactions between the emitted particles.

This work presents a status report of a STAR analysis of unlike-sign kaon femtoscopic correlation in Au+Au collisions at $\sqrt{s_{NN}}$=200 GeV, including the region of ϕ (1020) resonances, in which due to the strong final-state interaction will be sensitive to the source size. The experimental results are compared with HYDJET++ simulations and to a theoretical prediction that includes the treatment of resonance formation due to the final-state interactions.

Key words: Correlation femtoscopy, unlike-sign kaon correlation function, STAR experiment, HYDJET++, Lednicky model.

Název práce:
Femtoskopie neidentických kaonů na experimentu STAR

Autor: Jindřich Lidrych

Abstrakt:

Vysokoenergetické srážky těžkých iontů jsou klíčem ke studiu jaderné hmoty za extrémních podmínek. Očekává se, že během nich může dojít k vytvoření nové fáze jaderné hmoty, takzvaného kvark-gluonové plazmatu. Měření dvoučásticových korelací při malých relativních hybnostech poskytují informaci o časoprostorových rozměrech v okamžiku emise částic. Korelace jsou výsledkem kvantové statistiky, Coulombické interakce a silné interakce působící mezi emitovanými částicemi.

V této práci jsou prezentovány výsledky měření korelačních funkcí neidentických kaonů ze srážkách zlata při energii $\sqrt{s_{NN}}$=200 GeV na experimentu STAR. Tyto korelační funkce obsahují oblast resonance $\phi(1020)$, ve které jsou kvůli působení silné interakci ve finálním stavu ciltivé na velikost zdroje. Experimentální výsledky jsou porovnány se simulacemi z modelu HYDJET++ a s teoretickými předpovědmi, které obsahují přítomnost resonancí díky interakci ve finálním stavu.

Klíčová slova: Korelační femtoskopie, korelační funkce neidentických kaonů, STAR experiment, HYDJET++, Lednický model.

Acknowledgement

I would like to thank my supervisor, RNDr. Petr Chaloupka, Ph.D. for his patience, professional support and unvaluable help with my first analysis presented in this work.

Contents

List of Figures

List of Tables

Chapter 1

Femtoscopy

Femtoscopy, measurements of two particle correlations at small relative momenta, is a unique tool for measuring the space-time characteristics of the particle emitting source. In this chapter, we introduce a theoretical background of this technique known as femtoscopy and it will be shown its application in heavy ion collisions.

1.1 Historical background of femtoscopy

In 1950's Robert Hanbury Brown and Richard Q. Twiss invented a technique [1] allowing to measure space characteristics of stellar objects. This technique was based on measurement of the photon intensity interferometry.

A few years later, similar technique was used in particle physics by G.Goldhaber, S. Goldhaber, W.-Y. Lee and A. Pais [2]. They observed enhancement of identical pion pairs at low relative momentum, which were produced in proton-antiproton annihilation:

$$\bar{p} + p \to \pi^{\pm} + \pi^{\pm} + n\pi^{0} + \dots . \tag{1.1}$$

Observed correlations, as they correctly asserted, came from a quantum statistics.

However, the main share of developing the femtoscopy is owed to by Russian scientists and mathematics G. I. Kopylov and M. I. Podgoretsky, who explained that correlations are results of the fact that likelihood of emission of particle a with momentum p_a is modified by the emission of particle b with momentum p_b and two particle relative wave function $\psi(q, r)$, where $q = p_a - p_b$ is the relative momentum and r is the relative distance of particle a and b.

As a reference to R. Hanbury Brown, R. Q. Twiss and their pioneering in measurement of space-time structure, in femtoscopy we use terms like "HBT", "HBT radia" and so on.

1.2 Derivation of correlation function

Correlation function, as was derived for general case by Koonin and Pratt, can be expressed as

$$C\left(\vec{p_1},\vec{p_2}\right)=\int d^3rS\left(r,k^*\right)\left|\psi_{1,2}\left(r,k^*\right)\right|^2, \tag{1.2}$$

where $S\left(r,k\right)$ is source function describing emission of two particle in relative distance r with relative momentum $q=p_1-p_2=2k^*$. The interaction of these particle is encoded into two particle relative wave function $\psi_{1,2}\left(r,k^*\right)$.

In the following part of the section, we show derivation of two particle correlation function, but no so generally as previous one.

The probability to emit particle with four-momentum p from position x is characterized by single particle emission function $S(x,p)$ and by integration over the whole source

$$P(\vec{p})=\int d^4xS(x,p), \tag{1.3}$$

we can obtain the total probability $P(\vec{p})$. For two independent particles, the probability of emission of two particles with four-momentum p_1,p_2 from x_1,x_2 is

$$P(\vec{p_1})P(\vec{p_2})=\int d^4x_1d^4x_2S(x_1,p_1)S(x_2,p_2)=\int d^4x_1S(x_1,p_1)\int d^4x_2S(x_2,p_2). \tag{1.4}$$

Due to the fact that the emission of two particles from one source is connected via the wave function ψ reflecting their interaction, we have to calculate with it. Therefore, the previous term is modified into

$$P(\vec{p_1},\vec{p_2})=\int d^4x_1d^4x_2S(x_1,p_1)S(x_2,p_2)\left|\psi\left(\vec{q},\vec{r}\right)\right|^2. \tag{1.5}$$

Subsequently, one can define the correlation function as a ratio of the probability of emission of two particle and the probability of emission each particle. Experimentally the two particle correlation function is constructed as the ratio of the measured two particle inclusive spectra and single-particle inclusive spectra [3] i.e.:

$$\begin{aligned}C\left(\vec{p_1},\vec{p_2}\right)&=\frac{dN^{12}/\left(d^3p_1d^3p_2\right)}{\left(dN^1/d^3p_1\right)\left(dN^2/d^3p_2\right)}=\frac{P\left(\vec{p_1},\vec{p_2}\right)}{P\left(\vec{p_1}\right)P\left(\vec{p_2}\right)}=\\&=\frac{\int d^4x_1d^4x_2S(x_1,p_1)S(x_2,p_2)\left|\psi\left(\vec{q},\vec{r}\right)\right|^2}{\int d^4x_1S(x_1,p_1)\int d^4x_2S\left(x_2,p_2\right)}.\end{aligned} \tag{1.6}$$

For continuing in the derivation, we have to specify particle, with which we will work. Simpler case that can occur, it is a situation when identical particles do not interact. On the other hand, as shown in [4], [5], the calculation with interacting pacticles is more complicated, but not impossible.

1.2.1 Identical non-interacting particles

In case of non-interacting identical particles, we use a quantum statistics, namely Bose-Einstein statistics for bosons and Fermi-Dirac for fermions, for construction of the wave function that is then expressed as

$$\psi = \frac{1}{\sqrt{2}}\left[e^{i\left(x_1{}' - x_1\right)p_1} e^{i\left(x_2{}' - x_2\right)p_2} \pm e^{i\left(x_1{}' - x_2\right)p_1} e^{i\left(x_2{}' - x_1\right)p_2}\right], \tag{1.7}$$

where x_i is emission point and $x_i^{'}$ is point, where the particle were detected. According to the indistinguishable of particles, as the Fig. 1.1 shows, the wave function have to be either symmetric (sign +) for bosons or antisymmetric (sign -) for fermions respectively.

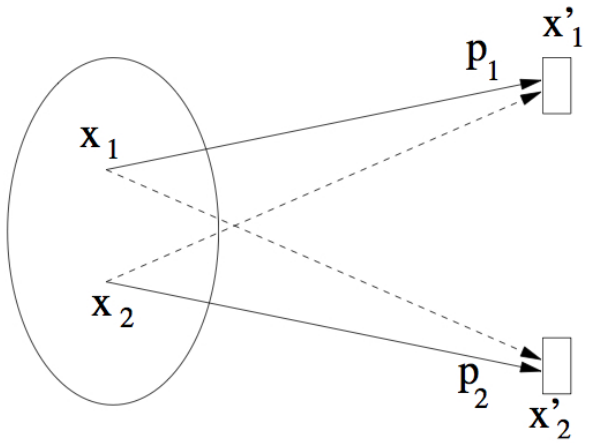

Fig. 1.1: The schema of source emitting particles. Taken from [6] .

By squaring this wave function and applying relations for the relative pair momentum q and the relative distance r, we can obtain

$$\begin{aligned} |\psi|^2 = \psi\psi^* = \frac{1}{2}\left(2 \pm 2\cos\left(\left(\vec{p_1} - \vec{p_2}\right)\left(\vec{x_1} - \vec{x_2}\right)\right)\right) = \\ = 1 \pm \cos\left(\left(\vec{p_1} - \vec{p_2}\right)\left(\vec{x_1} - \vec{x_2}\right)\right) = 1 \pm \cos\left(\vec{q}\cdot\vec{r}\right). \end{aligned} \tag{1.8}$$

As we will see subsequently, it is suitable to rewrite the emission source function into terms of the relative and average variables. Therefore we define the average pair momentum as

$$K = \frac{p_1 + p_2}{2} = \frac{P}{2}. \tag{1.9}$$

and the average pair position

$$x = \frac{1}{2}(x_1 + x_2) \tag{1.10}$$

respectively.

Thanks to these two expressions, the Eq. 1.5 is simplify into

$$\begin{aligned}
&\int d^4x_1 S\left(x_1,p_1\right) d^4x_2 S\left(x_2,p_2\right) \left|\psi\left(\vec{q},\vec{r}\right)\right|^2 = \\
&= \int d^4x d^4r S\left(x+\frac{r}{2},K+\frac{q}{2}\right) S\left(x-\frac{r}{2},K-\frac{q}{2}\right) \left|\psi\left(\vec{q},\vec{r}\right)\right|^2 = \\
&= \int d^4x d^4r S\left(x+\frac{r}{2},K\right) S\left(x-\frac{r}{2},K\right) \left|\psi\left(\vec{q},\vec{r}\right)\right|^2 = \\
&= \int d^4r \left|\psi\left(\vec{q},\vec{r}\right)\right|^2 \int d^4x S\left(x+\frac{r}{2},K\right) S\left(x-\frac{r}{2},K\right),
\end{aligned} \tag{1.11}$$

where we have just neglected the relative pair momentum. This approximation is *"the smoothness assumption"* and it is valid for small q.

Now, we rewrite the definition of the correlation function by putting this equation and the Eq. 1.8 into the Eq. 1.6 and we gain

$$\begin{aligned}
C\left(\vec{P},\vec{q}\right) &= 1 \pm \frac{\int d^4r \cos\left(\vec{q}\cdot\vec{r}\right) \int d^4x S\left(x+\frac{r}{2},K\right) S\left(x-\frac{r}{2},K\right)}{\left|\int d^4x S\left(x,K\right)\right|^2} = \\
&= 1 \pm \frac{\int d^3r \cos\left(\vec{q}\cdot\vec{r}\right) \int dt \int d^4x S\left(x+\frac{r+\vec{\beta}t,}{2},K\right) S\left(x-\frac{r+\vec{\beta}t,}{2},K\right)}{\left|\int d^4x S\left(x,K\right)\right|^2}.
\end{aligned} \tag{1.12}$$

Finally, we define the relative source function

$$S_{\vec{K}}\left(\vec{r}\right) = \int dt \int d^4x S\left(x+\frac{r+\vec{\beta}t,}{2},K\right) S\left(x-\frac{r+\vec{\beta}t,}{2},K\right) \tag{1.13}$$

and two particle correlation function arrives as

$$C\left(\vec{P},\vec{q}\right) = 1 \pm \frac{\int d^3r \cos\left(\vec{q}\cdot\vec{r}\right) S_{\vec{K}}\left(\vec{r}\right)}{\left|\int d^4x S\left(x,K\right)\right|^2}. \tag{1.14}$$

The last adjustments have been allowed by the fact that two emitted particles are on-shell and therefore components of q are not independent, but they are related by

$$q^0 = \vec{\beta}\cdot\vec{q}, \tag{1.15}$$

where

$$\vec{\beta} = \frac{\vec{K}}{K_0} \approx \frac{\vec{K}}{E_k}. \tag{1.16}$$

As can be seen, for identical non-interacting particles the correlation function is a Fourier transformation of the relative source function, into which the time information is convoluted. Hence the time-structure of the source is studied by comparison with the model describing four-dimensional particle emission.

From practical reasons, as the fitting, it is common to assume that the parametrization of single particle emission function has Gaussian form

$$S(x,p) = \frac{1}{\pi^2 R^3 \tau} e^{-\left(\frac{r}{R}\right)^2 - \left(\frac{t}{\tau}\right)^2}, \tag{1.17}$$

where R is the source radius and τ is the emission duration. In such a case, the Fourier transform exists and it is an analytical function

$$C(\vec{q}) = 1 \pm e^{-\vec{q}^2 R^2}. \tag{1.18}$$

The correlation function for different source size R is in the Fig. 1.2, where we have just used Bose-Einstein statistics (sign $+$).

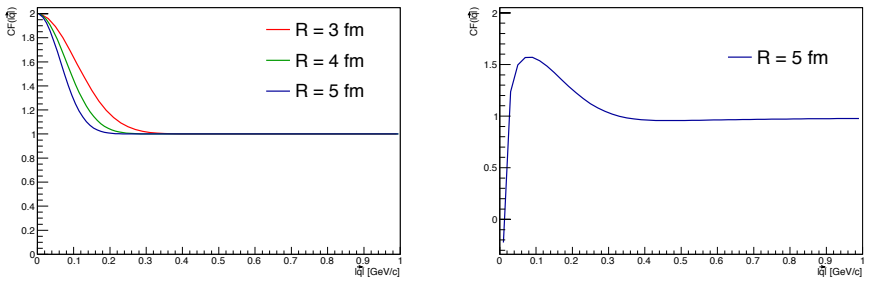

Fig. 1.2: L: the correlation function for non-interacting identical particles and for different source size R. R: the correlation function for like-sign particle.

1.2.2 Interacting particles

The previous derivation assumes non-interacting particles. However, in particle physics is more easy to measure charged particles. These particles feel attractive or repulsive potential of Coulomb interaction. As a result of this interaction, we observe a suppression, or enhancement, of the measured like-sign, or unlike-sign respectively, two particle correlation function at low $\vec{q}$, as the Fig. 1.2 illustrates. The Fig. 1.2 shows a correlation function, which is constructed for like-sign pair described by Bose-Einstein statistics and Coulomb interaction.

There is also a strong interaction between emitted particles, especially unlike-sign pairs. The derivation of the correlation function, which take into account all these effect, can be found in [4], [5].

1.3 Coordinate system

According to typical symmetry, the classical Cartesian system is not optimal. The most common one for femtoscopy is the Bertsch-Pratt coordinate system

[3]. The Bertsch-Pratt coordinate system, sometimes named as "out-side-long system", is connected with emitted pair of particles and it is characterized by three axis, namely longitudinal, outward and sideward axis. The longitudinal axis is parallel to the beam - typically in laboratory system z-axis. The direction of the outward axis is parallel to pair transverse momentum k_T. The last axis, the sideward axis, is chosen so that it would be perpendicular to the longitudinal and outward axes. Into this coordinate system, components of each four vector V are transformed:

$$\begin{aligned} V_{long} &= V_z \\ V_{out} &= \left(P_x V_x + P_y V_y\right)/P_T \\ V_{side} &= \left(P_x V_y - P_y V_x\right)/P_T \end{aligned} \tag{1.19}$$

where $P = (P_0, P_x, P_y, P_z)$ is pair momentum.

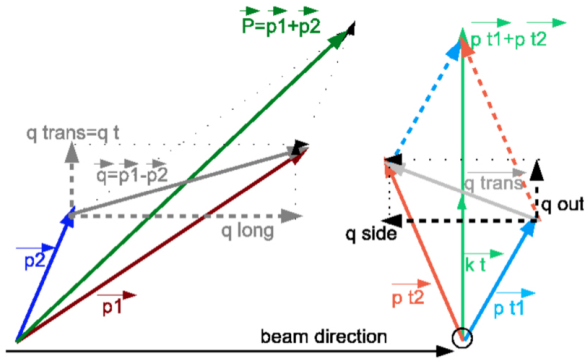

Fig. 1.3: The Bertsch-Pratt coordinate system. Taken from [5] .

For the femtoscopy with non-identical particles, the pair's rest frame (PRF) is the most suitable. In PRF, each particle has the same momentum

$$\vec{k^*} = \vec{k_1} = -\vec{k_2} \tag{1.20}$$

and hence the relative pair momentum is

$$\vec{q} = 2\vec{k^*}. \tag{1.21}$$

1.4 Parametrization of correlation function

To extract information from the measurement, we have to parametrized experimentally constructed correlation function and the emission function. The easiest parametrization of the single particle emission function, as shown by the Eq. 1.17, is Gaussian. Although it is known that real sources, especially pion

source, deviate from Gaussian. Observed deviation is ascribed to resonance decay, which cause the exponential tails. By using Gaussian parametrization, then the one-dimensional correlation function is expressed as

$$C(q_{inv}, \vec{K}) = 1 + \lambda(q_{inv}) \exp\left(-q_{inv}^2 R_{inv}^2(\vec{K})\right), \tag{1.22}$$

where λ is the lambda parameter, R_{inv} is the source radius and q_{inv} defined as

$$q_{inv} = \sqrt{(E_1 - E_2)^2 - (\vec{p_1} - \vec{p_2})^2}. \tag{1.23}$$

The three-dimensional correlation function in case of the absence of an information about the event plane is

$$C(\vec{q}, \vec{K}) = 1 + \lambda(\vec{K}) \exp\left(-R_o^2(\vec{K}) q_o^2 - R_s^2(\vec{K}) q_s^2 - R_l^2(\vec{K}) q_l^2\right). \tag{1.24}$$

1.4.1 λ parameter

The lambda parameter, sometimes called as the incoherence factor, contains information about all imperfections, which happens during the measurement of the correlation function. These imprecisions, like misidentified particles as well as admixture of particles coming from resonance decay, cause that measured correlation function is smaller then the theoretical function and hence the lambda parameter was introduce to compensate their influence. For ideal case, the lambda parameter is equal to unity.

1.5 HBT radii and model predictions

The expansion and space-time evolution of the measured source cause the collective flow, which produced the correlation of the total momentum of the pair and position of the emission, noted as x-p correlations. The information about the dynamic structure of the source is encoded into the correlation function and therefore the measured R_{out}, R_{side} and R_{long}, known as HBT radii, can not be simply identified as the sizes of the whole system. The HBT radii depend on the total momentum of the pair and measure the size of the regions emitting particles, called as *"homogeneity region"*. The different size of the homogeneity region for various transverse pair momentum k_T, as is shown in the Fig. 1.4, is a result of *"the thermal smearing effect"* [7].

The thermal smearing effect is caused by superposition of thermal motion with radial motion. Without the thermal motion all particles with the same momentum vector would be emitted from the same spatial point. However the thermal motion smears the point-like emission and create a larger homogeneity region. The strength of this effect depends on particle mass as well as its velocity. The lighter particles in comparison with the heavier ones are smeared more over the volume of the source as is illustrated in the Fig. 1.5. The mean emission point is shifted from the center and the magnitude of the shift increases with m_T.

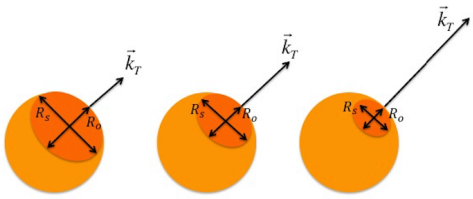

Fig. 1.4: Homogeneity region for different pair transverse momenta.

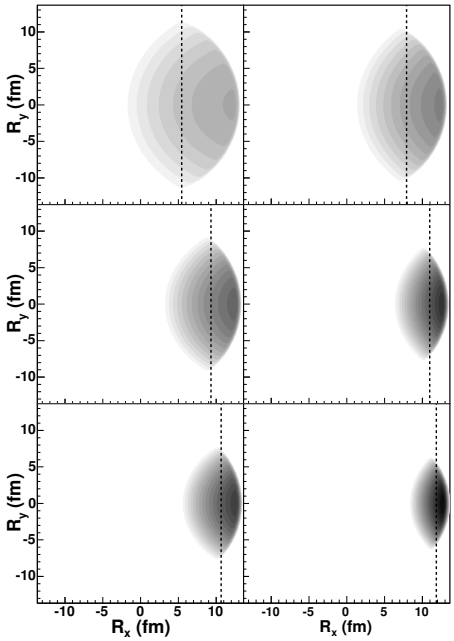

Fig. 1.5: The homogeneity region - the top panel is pion, the middle panel is for kaons and botton for proton. Left-hand side is for $\beta_x = 0.907$ and the right-hand side is for $\beta_x = 0.974$. Taken from [7].

The evidence of such behavior, we can observe on falling the R_{out}. The similar behavior, which is caused by the longitudinal flow, is observe on falling the R_{long} with p_T as $1/\sqrt{m_T}$, which is shown in the Fig. 1.6. This data set was made from the existing measurement of the pion radii by different experiments at the AGS, SPS and RHIC.

For these measurement data were used from the most central Au+Au or Pb+Pb collisions. As can be seen from the Fig. 1.6, for different energies, which change over two orders, the m_T dependence of R_l is surprisingly the same.

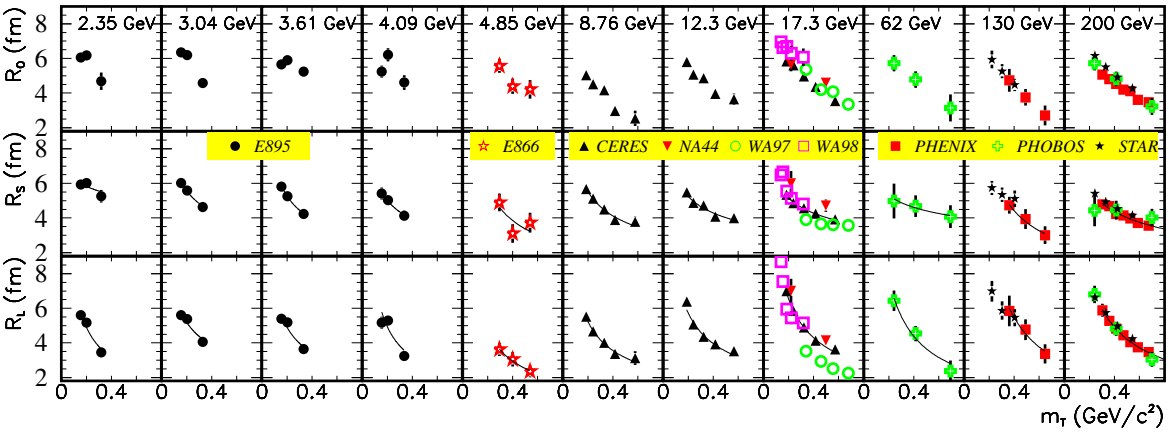

Fig. 1.6: World data set m_T dependence of HBT parameters. Taken from [3].

For this reason, to obtain complete information about the source, except measuring the HBT radii we have to compare of them to models of the heavy-ion collisions. In femtoscopy it is common to use a family of simplified models which use hydro-inspired parametrization of the particle emitting source. There are many such models. One of the most commonly used is the blast wave model [7] of Retiere and Lisa. Some of them can be quite sophisticated, including such effects like resonance and particle decay. Example of this model, can be a HYDJET++ [8], which is also used for analysis presented in this work.

1.5.1 HYDJET++

HYDJET++ (HYDrodynamics plus JETs) is Monte Carlo heavy ion event generator for simulation of relativistic heavy ion AA collisions [8]. It is considered as a superposition of the soft, hydro-type state and the hard state resulting from multi-parton fragmentation. The soft part of HYDJET++ is based on the parameterization of relativistic hydrodynamics with present freeze-out conditions used for the chemical and thermal freeze-out hypersurfaces during generating the thermal hadronic state. HYDJET++ includes the longitudinal, radial and elliptic flow effect ant the decays of hadronic resonances. HYDJET++ have been successfully tuned for description of Au+Au collisions at $\sqrt{s_{NN}}$=200 GeV as well as for collisions at energy reached in LHC. As a example, we can shown the comparison of particle ratios from HYDJET++ with the experimental data shown in the Fig. 1.7.

The decays of the resonance allows to study the effect of non-primary particle on the relative space-time shift as shown in the Fig. 1.8, where the measured HBT radii from $\pi-\pi$ correlation are compared to theoretical from HYDJET++.

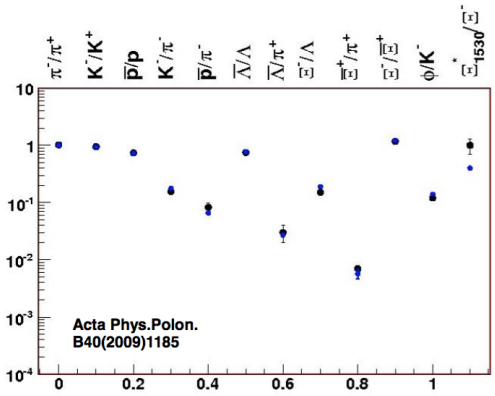

Fig. 1.7: The particle number ratios from HYDJET++ (blue points) compared with the experimental data (black points). Taken from [8].

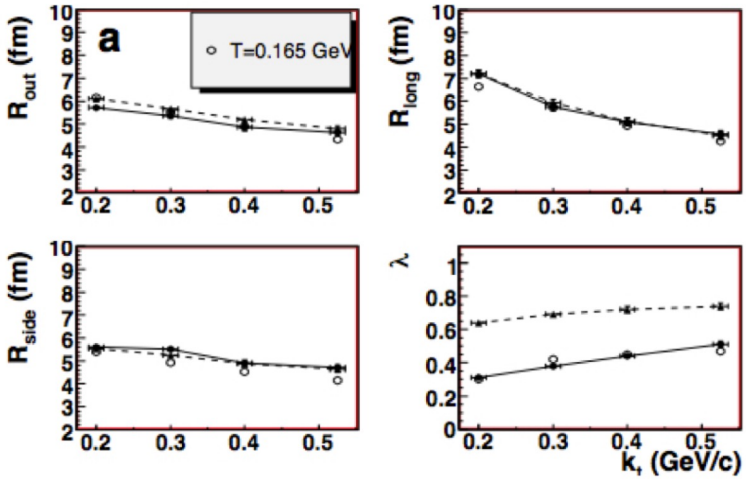

Fig. 1.8: The HBT radii from $\pi^+\pi^+$ correlation function for central Au+Au collisions (open circles) and results from HYDJET++: no weak decays(dashed line), with weak decays (solid line). Taken from [9].

1.6 Experimental correlation function

Experimentally, the correlation function is constructed as the ratio of two-particle distributions:

$$C(\vec{q}) = N\frac{A(\vec{q})}{B(\vec{q})} = \frac{real\ pair}{mixed\ pair}. \tag{1.25}$$

The numerator, $A(\vec{q})$, is two-particle distribution obtained from the single events. On the other hand, the denominator, $B(\vec{q})$ is two-particle distribution formed from the event mixing procedure. By using this procedure, we remove non-femtoscopis correlations, since each particle in the pair comes from different event. Finally, the correlation function have to be normalized to unity. The normalization N is calculated in region, where we do not observe correlation effects.

Chapter 2

Kaon femtoscopy

In this chapter, we present motivation for unlike-sign kaon femtoscopy. Also previous results from like-sign kaon correlation measurement will be introduced.

2.1 Motivation for unlike-sign kaon femtoscopy

In standard HBT measurement we study correlation function, which as shown in previous chapter, reflects particle emission source and two-particle interaction described by wave function. The correlations result from quantum statistics, final-state Coulomb interactions, and the strong final-state interactions (FSI) between the emitted particles. The formalism is well establish for region of low q_{inv}, where we observe these correlations.

The idea of this analysis is try to use the region of higher q_{inv} in the system where narrow resonance is presented. As has been predicted [4], that the correlations due to the strong FSI will be sensitive in region of the resonance the source size and momentum-space correlations. Such a measurement can provide complementary information to the measurements at the very low relative momenta. Even these measurement will be more statistically advantageous, it also brings challenges as possibility of break-down of basic assumptions like smoothness assumption as well as equal-time approximation.

The systems of unlike-sign kaon and unlike-sign $\pi - \Xi$ pairs are ideally suited for testing this extension of femtoscopy formalism as it contains narrow $\phi(1020)$ resonance, $\Xi^*(1530)$ resonance respectively.

The femtoscopy with $\pi - \Xi$ has been already performed [5]. However these measurements were done with statistics from year 2004 and therefore the results were statistically challenged as shown in the Fig. 2.1.

The main advantageous of this analysis will be higher available statistics. Also there will be cleaner probe of the emitting source due to smaller contaminations from the resonance decays compared with pions. Therefore the kaon source function is better parametrized by the Gaussian as shown in the Fig. 2.2, where the kaon source function is compared to pion emission function. As we

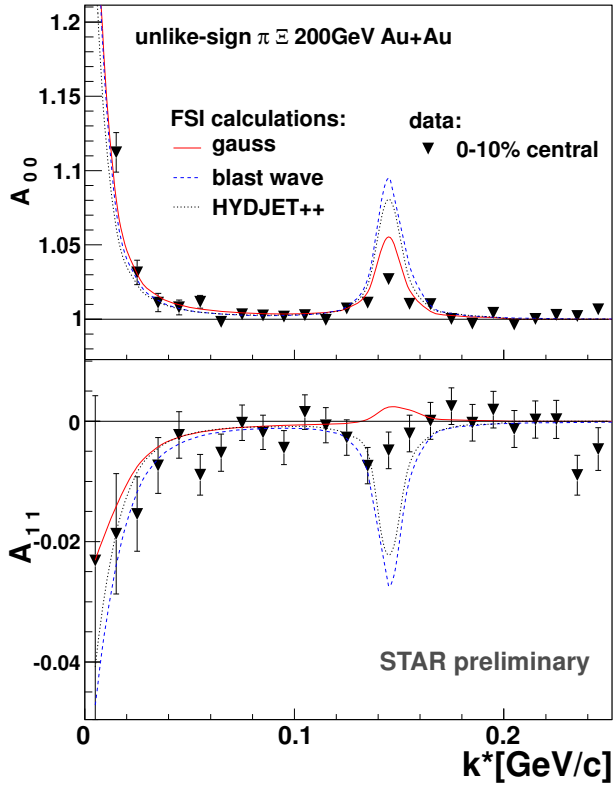

Fig. 2.1: Experimental $\pi-\Xi$ correlation function decomposed into spherical harmonics compared to FSI calculations with gauss, blast wave and HYDJET++. Taken from [5].

can see on pion emission function, the resonance decays cause exponential tails and hence the Gaussian parametrization is insufficient. It should be also noted, that STAR extracted the HBT radii from like-sign correlation, which are also shown in the Fig. 2.2. Even the kaon analysis was done with different k_T bins and centralities than we plan to use in our analysis, results of them can be used as reference for us.

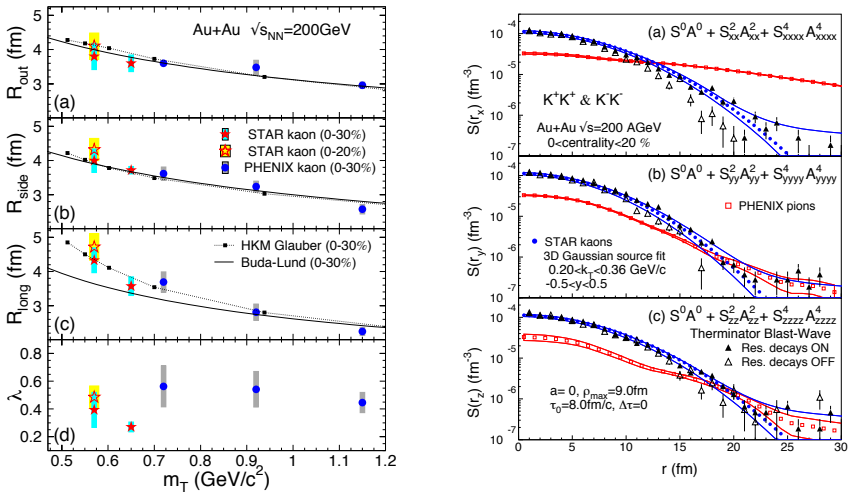

Fig. 2.2: L: HBT radii obtained with kaon femtoscopy from STAR experiment are compared to results from Phenix. R: Kaon emission source function is compare to pion emission function. Taken from [10].

Chapter 3

Analysis

A detailed description of the analysis is given in this chapter. Consecutively we introduce selection criteria, cuts and methods used in this analysis.

3.1 Data sample

For this analysis, we use data sample noted as *vpd-zdc-mb-protected* which was recorded during Au+Au collisions at $\sqrt{s_{NN}}$=200 GeV in 2011 by the STAR experiment. The minimum bias collisions were triggered by using VPD and ZDC detectors with offline trigger ID: 350003, 350013, 350023, 350033 and 350043. The total number of available events for analysis is 730.94 million.

Due to the fact that the development of analysis software is underway and we use a raw data, which are saved in MuDst files and to analyze them can take up to a few weeks, the presented results were obtain by using ∼400 million events.

3.2 Event selection and centrality binning

Firstly, we apply event cut to select only collision which takes place in the middle of the detector in order to keep the same detector acceptance. Therefore, the vertex z position (along the beam axis) has to be smaller than 30 cm from the center of TPC.

Even thought the data sample is noted as *protected* and so the effects of the pile-up should be remove, we require in order that the difference between the vertex reconstruction from TPC and VPD would be smaller than 5 cm. The phenomenon pile-up occurs when there is small time difference between two collisions and not all particles from the first collision have yet leave the detector.

The Fig. 3.1 shows these two selection criteria applied on the data sample. As we can see, the majority of the events fulfill these cuts.

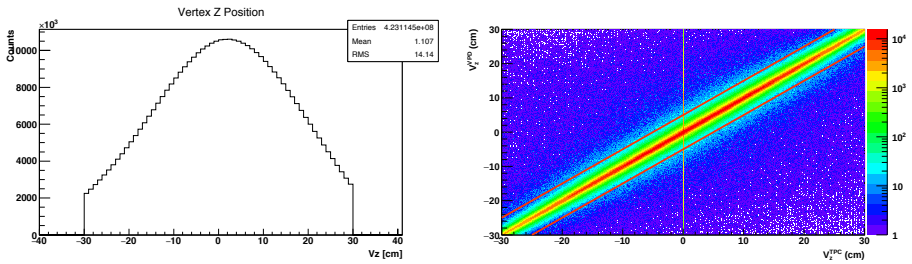

Fig. 3.1: Left: distribution of the vertex z position after cut. Right: distribution of the vertex z position reconstructed by the TPC and VPD before cut. Red lines represent used cut.

There is no way how to measure the impact parameter directly and so we must try to obtain information about the centrality from the measured multiplicity of charged hadrons. The raw data contains *uncorrected reference multiplicity* and to each value of the uncorrected reference multiplicity we assign the centrality of the collisions. To more precise determine the centrality, we would have to calcule the *corrected multiplicity*, which is non-trivial function of the *uncorrected reference multiplicity*, vertex z position and ZDC coincidence. It also depends on seven parameters and their value have to be experimentally measured for each run number and reflect the detector acceptance in given period.

The definition of the corresponding centrality to given multiplicity is based on Glauber model simulations and is shown in the Fig. 3.2.

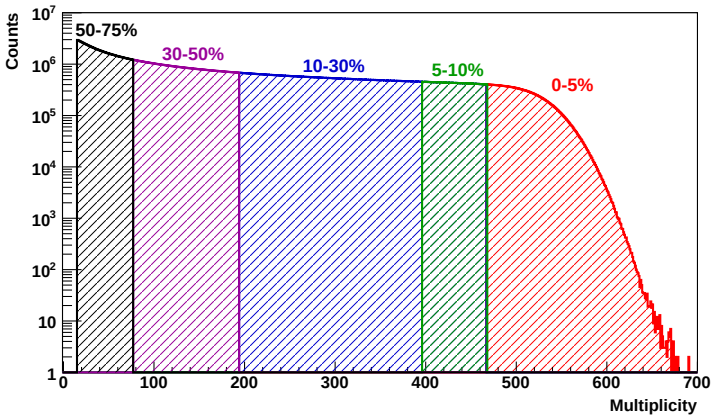

Fig. 3.2: The multiplicity distribution and corresponding centrality.

As was mentioned in previous chapter, for constructing correlation function, we have to obtain uncorrelated two-particle distributions. In this analysis, mixed pairs are calculated so that each particle from one event is mixed with all particles from the sub-classes of similar events. Each classes contains 10 events and classification is done according to vertex z position and multiplicity. We use 10 bins for dividing distribution of primary vertex position (1 bin per 3 cm) and 7 bins for the multiplicity distribution (1 bin per 100). This used mixing procedure allows us to remove all non-femtoscopics correlations.

3.3 Track selection

From the events which passed the previous mentioned cuts, we can select suitable tracks. The tracking is done by using the TPC detector.

We selected the tracks in the pseudorapidity region $|\eta| < 1$ with number of hits used for fitting the track shape nHitsFit$\geq$15. To reduce contribution from non-primary kaons, we applied a DCA cut. Track, which has distance of closest approach of the extrapolated track to the primary vertex smaller than 3 cm can fulfill this cut. The application of these cuts is shown in the Fig. 3.3.

The last cuts, which were used are on transverse momentum p_T. Only track with $p_T > 0.15$ GeV/c and with momentum $p > 0.15$ GeV/c are selected.

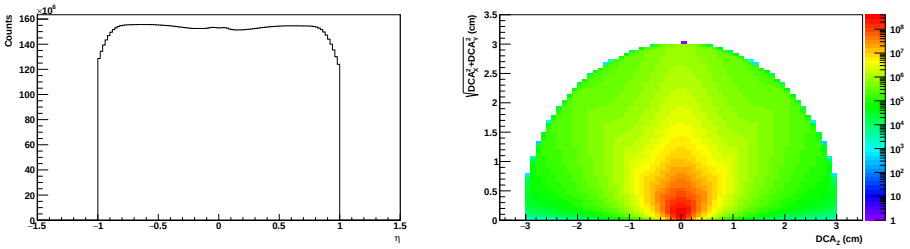

Fig. 3.3: Left: distribution of the pseudorapidity. Right: distribution of the DCA.

3.4 Kaon identification

The cuts described above were used for selection of quality tracks. Now, we need to apply cuts for particle identification, in our case kaon identification. The main subdetectors used in analysis presented in this work are TPC and ToF. Especially ToF is very precise to kaon identification since it allows to separate of charged kaons from other hadrons up to momentum $\sim$1.5 GeV/c.

3.4.1 nSigma cut

Besides of tracking, the TPC is also using for calculation of the specific ionization loss dE/dx. The energy lost by a particle as it travels through a given gas is described by the Bethe-Bloch formula. For a given momentum, each particle species (different mass) will have a different velocity and a different dE/dx. Due to this fact, we can identify particle as is shown in the Fig. 3.4.

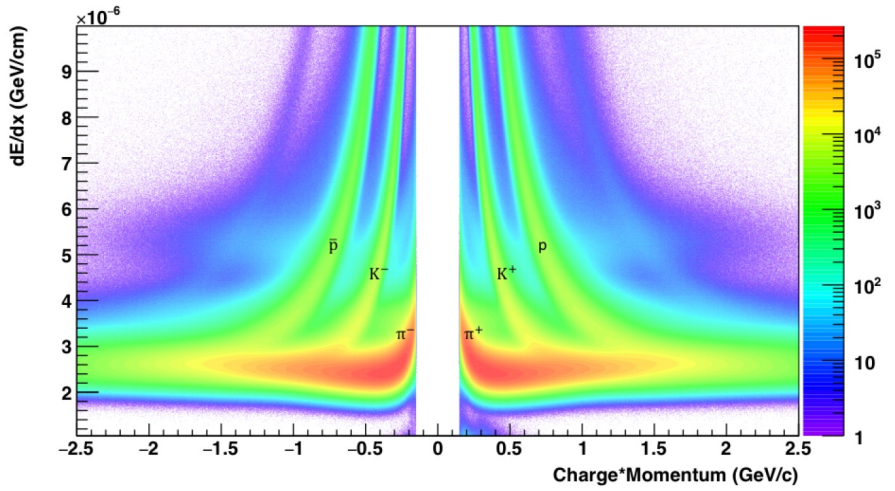

Fig. 3.4: dE/dx of charged particles measured by TPC.

We suppose that measured distribution of the energy loss, dE/dx^{meas}, has a Gaussian shape with a mean value described by theoretical value of dE/dx^{theo} and standard deviation unit σ. In our analysis we use nσ cut defined as

$$n\sigma = \frac{\ln\left(\frac{dE/dx^{meas}}{dE/dx^{theo}}\right)}{\sigma_{dE/dx}}. \tag{3.1}$$

By applying of this cut, we are able to eliminate particles, which do not lay in given distance from the expected dE/dx expressed in terms of σ. In our case, we require $|n\sigma_K|<3$. The Fig. 3.5 shows the distribution of nσ_K versus momentum. As can be seen, in higher p there is significant contaminations of pions and protons.

3.4.2 cut with ToF

In our analysis, the ToF is the most important detector for kaon identification. With the ToF, we can measure relative particle velocity β and it gives us to opportunity to separate of charged kaons of other hadrons and electrons up to

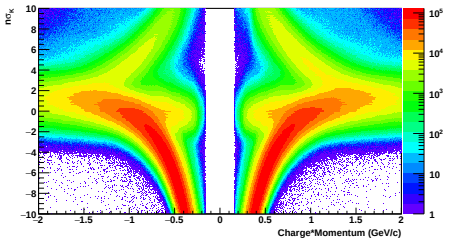

Fig. 3.5: Distribution of $n\sigma_K$ vs momentum p.

momentum ∼1.55 GeV/c as is shown in the Fig. 3.6. And therefore we have to focus on track with signal from the ToF and momentum $p < 1.55$ GeV/c.

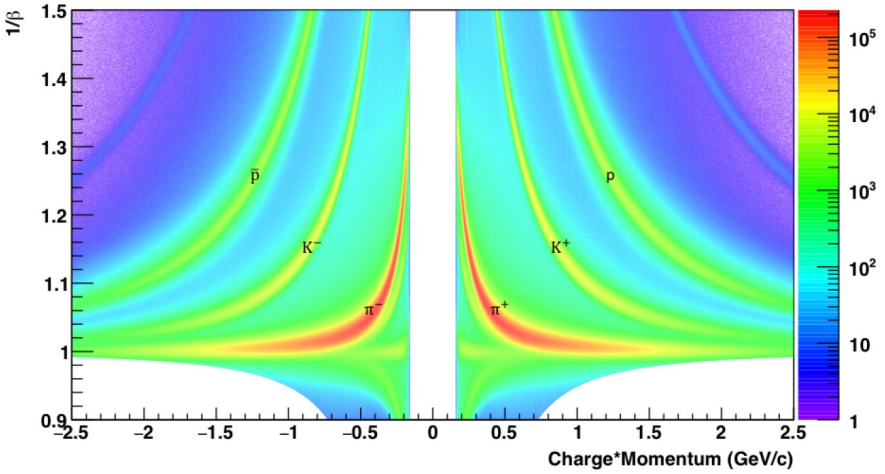

Fig. 3.6: $1/\beta$ of charged particles measured by ToF.

The measured relative particle velocity is consequently used for calculation of particle mass m according to the relation

$$\frac{1}{\beta} = \sqrt{1 + m^2/p^2}, \tag{3.2}$$

where p is measured by the TPC. The kaon mass is $m_K = 0.493667$ GeV/c^2, $m_K^2 = 0.243707$ GeV$^2/c^4$ respectively. Thus only particle with $0.21 < m^2 < 0.28$ GeV$^2/c^4$ can fulfill our last selection criteria.

This cut helps us to distinguish between kaons and other hadrons as is illustrated by the Fig. 3.7 and we can obtain very clean kaon sample.

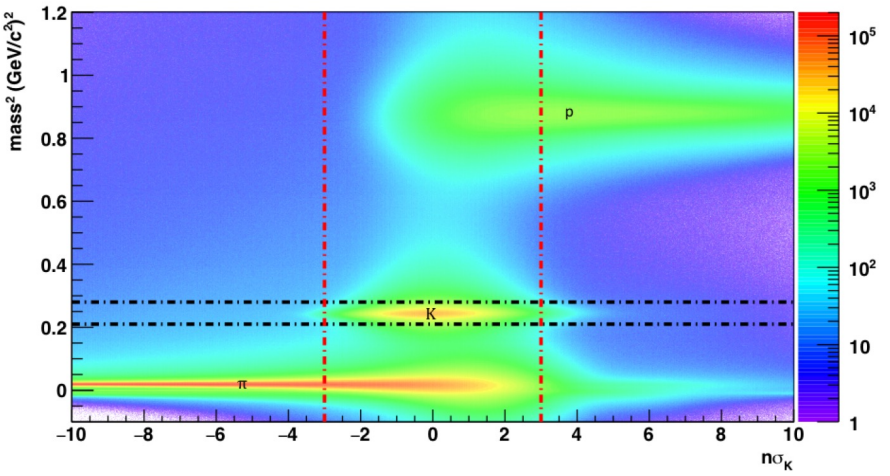

Fig. 3.7: Distribution of mass square of particle vs $n\sigma_K$. Red lines represent $n\sigma_K$ cut and black lines represent cut on particle mass.

3.5 Pair cut

Even with a clean kaon sample the two particle distribution contains detectors effect arise from the tracking imperfection, which shows up at low relative momentum q_{inv} of measured correlation function. These effects are track splitting and track merging. In following subsections, we describe way how to remove them.

3.5.1 Track splitting

A case, when one single particle is reconstructed as two track, is called as the track splitting [6] and it causes an enhancement of pairs at low relative momentum q_{inv}. To remove these split tracks we have to compare the location of the hits for each track in the pair in the pad-rows in the TPC and to assign a value of "splitting level" (SL) calculated as:

$$SL = \frac{\sum_i S_i}{Nhits_1 + Nhits_2}, \tag{3.3}$$

where

$$S_i = \begin{cases} +1 \ldots \text{one track leaves a hit on pad-row} \\ \text{-1} \ldots \text{both tracks leave a hit on pad-row} \\ 0 \ldots \text{neither track leaves a hit on pad-row,} \end{cases} \tag{3.4}$$

where i is the pad-row number of the TPC, and $NHits_1$ and $NHits_2$ are the total number of hits associated to each track in the pair. The SL ranges from

-0.5 to 1. The value -0.5 corresponds for certainly distinct two tracks. On the other hand, if the quality of pair is equal to 1, it is possible split track. The principle of this antisplitting cut is shown in the Fig. 3.8, where the four different cases are presented.

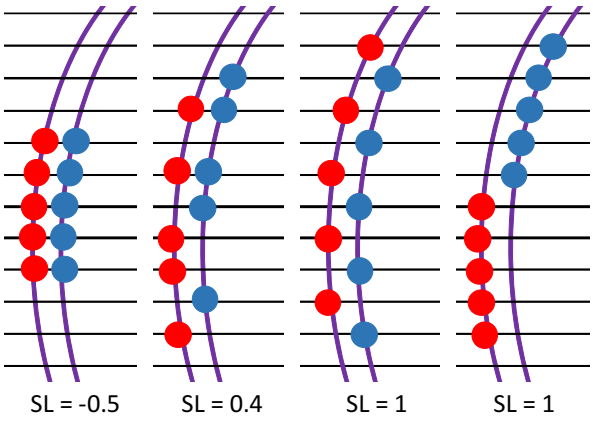

Fig. 3.8: Description of the anti-splitting cut, which shows four possible cases. Red circles are hits assigned to one track, blue circles are assigned to the other.

To remove these split tracks, we have to require each pair has SL smaller than a certain value. This value is experimentally determined from the correlation function constructed for different SL, which are shown in the Fig. 3.9, where the correlation functions for like-sign pair are. However we do not observe the effect of the track splitting. As a cross-check of no presence of track splitting, we can look at the distribution of pairs vs relative momentum q_{inv} and splitting level shown in the Fig. 3.10. In case that the correlation function should be influent by the track splitting, we should have to observe enhancement of pairs at low relative momentum and higher SL.

One of possible explanation of none track splitting can be that these tracks were already eliminated by previous track cuts. In case we replace $NHitsFit$ cut by $NHits$ cut, the situation is similar. Therefore, the major share on no presence of track splitting is assign to criteria on signal from ToF.

Even we do not observe track splitting, so according to available high statistics we can apply "standard" cut and SL$<$0.6 will be required.

3.5.2 Track merging

Besides of track splitting, it can happen two particles with similar momenta are reconstructed as one track. Merged tracks cause a reduction of pairs at

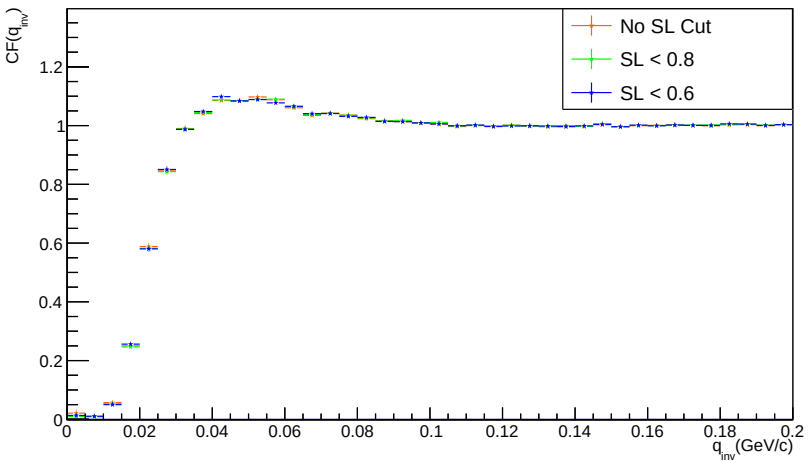

Fig. 3.9: One dimensional like-sign correlation function for different values of SL.

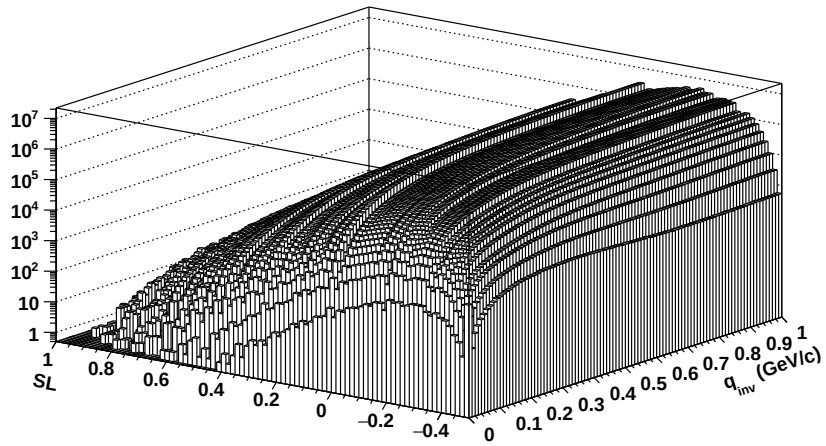

Fig. 3.10: Distribution of real pairs vs relative momentum q_{inv} and splitting level SL.

low relative momentum. Two hits are considered merged when the probability of separating them is less than 99% according to the two-track resolution in the TPC [6]. As was experimentally proved, to completed remove effect of track merging, we have to required of all pairs to have a fraction of merged hits smaller than 10%.

3.6 k_T cut

The last cut, which we have done, is cut on the average pair transverse momentum k_T, which is defined as

$$\vec{k_T} = \left(\frac{\vec{p_1} + \vec{p_2}}{2} \right)_T . \tag{3.5}$$

With this cut, we can chance the size of measured volume, homogeneity region and hence probe the dynamics of the system, during the constant centrality as was already mentioned and described in the Fig. 1.4. In our analysis, we require to have pairs with average transverse momentum between 0.05 and 1.25 GeV/c and they were divided in 4 k_T bins: 0.05-0.35, 0.35-0.65, 0.65-0.95 and 0.95-1.25 GeV/c. The Fig.3.11 shows a k_T distribution of real pairs.

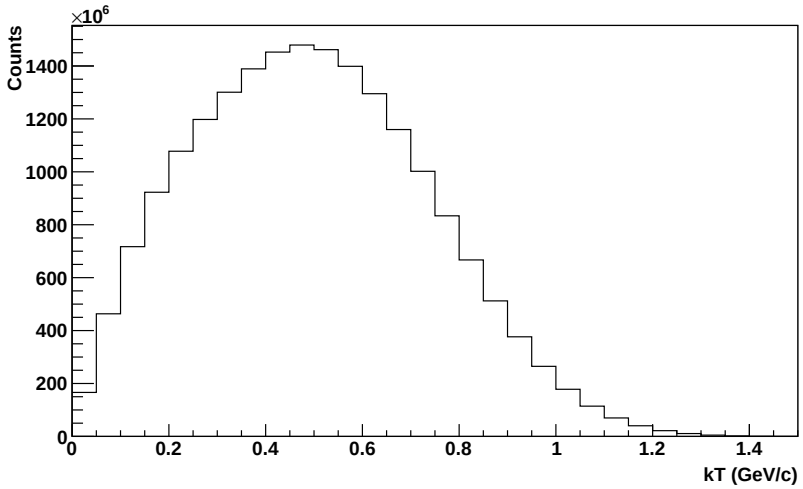

Fig. 3.11: k_T distribution of real pairs.

3.7 Overview of applied cuts and binning

For clarify, in Table 3.1 one can found the overview of applied cuts with brief description. The Table 3.2 and 3.3 contain the overview of used binning for

event mixing procedure and construction of correlation function.

Selection criteria	Description of selection criteria
Event cut	
$\lvert V_Z \rvert < 30$ cm	Position of event vertex in the beam direction
$\left\lvert V_Z^{TPC} - V_Z^{VPD} \right\rvert < 5$ cm	Difference between the vertex z position reconstruceted by TPC and VPD
Track cut	
$\lvert \eta \rvert < 1$	Selection of acceptance in pseudorapidity
nHitsFit > 15	Number of hits in TPC gas
$\lvert DCA \rvert < 3$ cm	Distance of closest approach of a track to the primary vertex pozition
$p_T > 0.15$ GeV/c	Transverse momentum of the track
$p > 0.15$ GeV/c	Momentum of the track
Kaon identification	
ToF	Required signal from the ToF
$p < 1.55$ GeV/c	Momentum of kaon
$\lvert n\sigma_K \rvert < 3$	Distance from the expected dE/dx for kaons in terms of standard deviation units
$0.21 < m^2 < 0.28$ GeV$^2/c^4$	Mass of kaon
Pair cut	
-0.5 < SL < 0.6	Split level
track merging	No more than 10% of merged track

Table 3.1: The overview of used selection criteria.

Binning for event mixing	
V_Z	10 bins per 3 cm
Multiplicity	7 bins per 100

Table 3.2: The overview of applied binning for event mixing procedure.

Binning for correlation function	
5 centralities	0-5%, 5-10%, 10-30%, 30-50%, 50-75%
4 k_T	0.05-0.35, 0.35-0.65, 0.65-0.95, 0.95-1.25 GeV/c

Table 3.3: The overview of used binning for construction of correlation function.

Chapter 4

Results

Using cuts and procedures described in the previous chapter we have obtained correlation functions for like-sing and unlike-sign pair of kaons. In this chapter the one dimensional correlation function for the 4 different k_T bins and 5 different centralities are presented. Also extraction of λ parameter and source radii R_{inv} from fitting like-sign correlation function will be shown. With these parameters, we will be able to compare of unlike-sign correlation function with models and study centrality and k_T dependence in region of the $\phi(1020)$ resonance.

4.1 Like-sign correlation function

As already discussed in chapter 1, the correlation function is sensitive to the sizes of the homogeneity regions. The size of these regions depends on the centrality of the collisions as is shown in the Fig. 4.1, where the like-sign correlation functions for different centralities are. These function are integrated over all k_T bins. At low relative momentum q_{inv}, we can observe the superposition of Bose - Einstein statistics and repulsive Coulomb interaction.

For the most central collisions, the source is the largest and kaons are emitted at a greater relative distance from each other. Hence the repulsive Coulomb interaction acting at low relative momentum q_{inv} is weaker. On the other hand, for peripheral collisions, the size of source is smaller. Therefore the particle are emitted closest to each other and more feel the repulsive potential of Coulomb interaction. In such case, at very low q_{inv} Bose - Einstein statistics, which is proportional to $1/R_{inv}$, is pressed by Coulomb interaction.

Also, the size of the homogeneity regions can be controlled by the transverse momenta of the pairs k_T entering into the correlation function. With increasing k_T, the homogeneity lengths is getting smaller. The k_T dependence of like-sign correlation function is presented in the Fig. 4.2, where the correlation function are measured for one centrality, but k_T dependence is observed for all centrality bins.

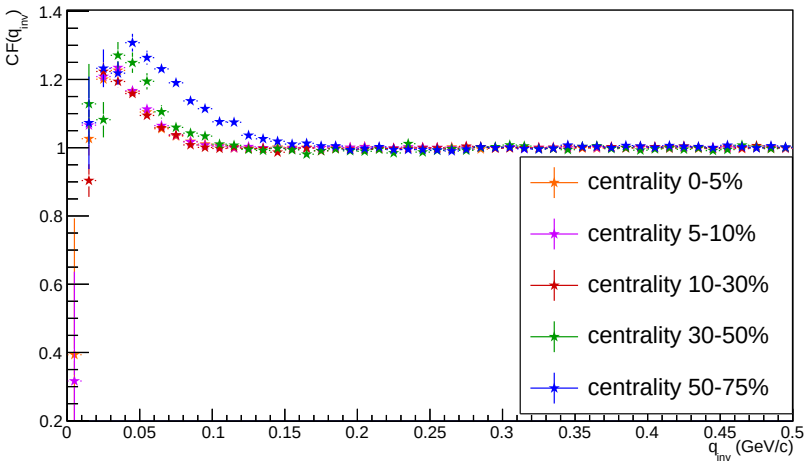

Fig. 4.1: One dimensional like-sign correlation function for different centralities.

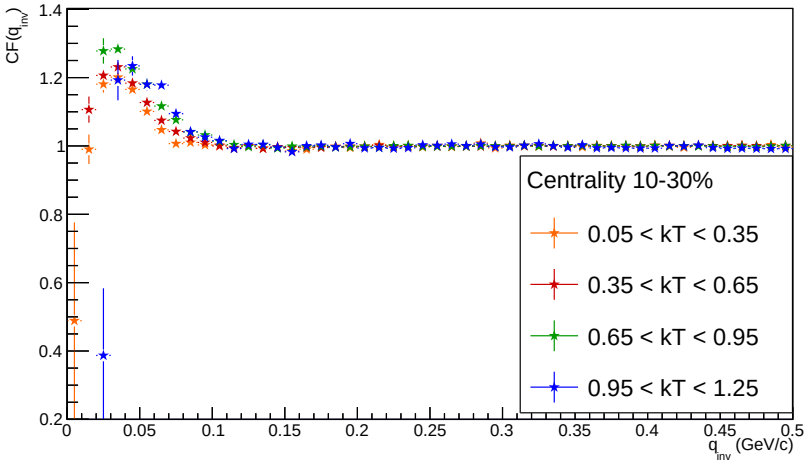

Fig. 4.2: One dimensional like-sign correlation function for different k_T bins and for centrality 10-30%.

4.2 Extraction of λ parameter and source radii R_{inv} from like-sign correlation function

Experimental correlation function contains correlations, which are results of the Coulomb interaction and therefore the fitting function is no the same as the one presented by the Eq. 1.18. To remove these effect, the experimental correlation functions were fitted by

$$CF(q_{inv}) = \left[(1-\lambda) + \lambda K\left(q_{inv}\right) \exp\left(-q_{inv}^2 R_{inv}^2\right)\right] N, \tag{4.1}$$

where $K(q_{inv})$ is the Coulomb function integrated over a spherical source of size corresponding the source radius R_{inv}, which is free parameter during fitting. Other free parameters are normalization factor N and λ parameter.

By this method, the K^+K^+ as well as K^-K^- correlation function were fitted and source radii R_{inv}, λ parameter and normalization N extracted as can be seen in the Fig. 4.3 and the Fig. 4.4, respectively.

The Fig. 4.4 shows that in both cases the measured source radii R_{inv} increase with the centrality and decrease with pair transverse momentum k_T as we expected. Difference between obtained value of source radii from K^+K^+ and K^-K^- correlation function, especially in the most central collisions, can be caused by the higher contaminations of electrons in K^-K^-.

The previous measurement of like-sign correlation function [10], which is discussed in chapter 4, was done for different centralities and different k_T bins, hence the comparison of our results with them is little complicated. But we can make conclusion that there is a good agreement.

In the Fig. 4.4 we also see how measured λ parameter changes with increasing transverse pair momentum k_T. In the most cases, λ parameter reaches maximum for k_T between 0.35 and 0.65 GeV/c.

Even when we have used very clean kaon sample, the measured value of λ parameter is around 0.6 . A weakening of correlation strength is therefore ascribe to admixture of no-primary kaons, which are not correlated. For better understanding of behavior of λ parameter, which is not trivial, in future we will use more k_T bins as well as stricter DCA cut.

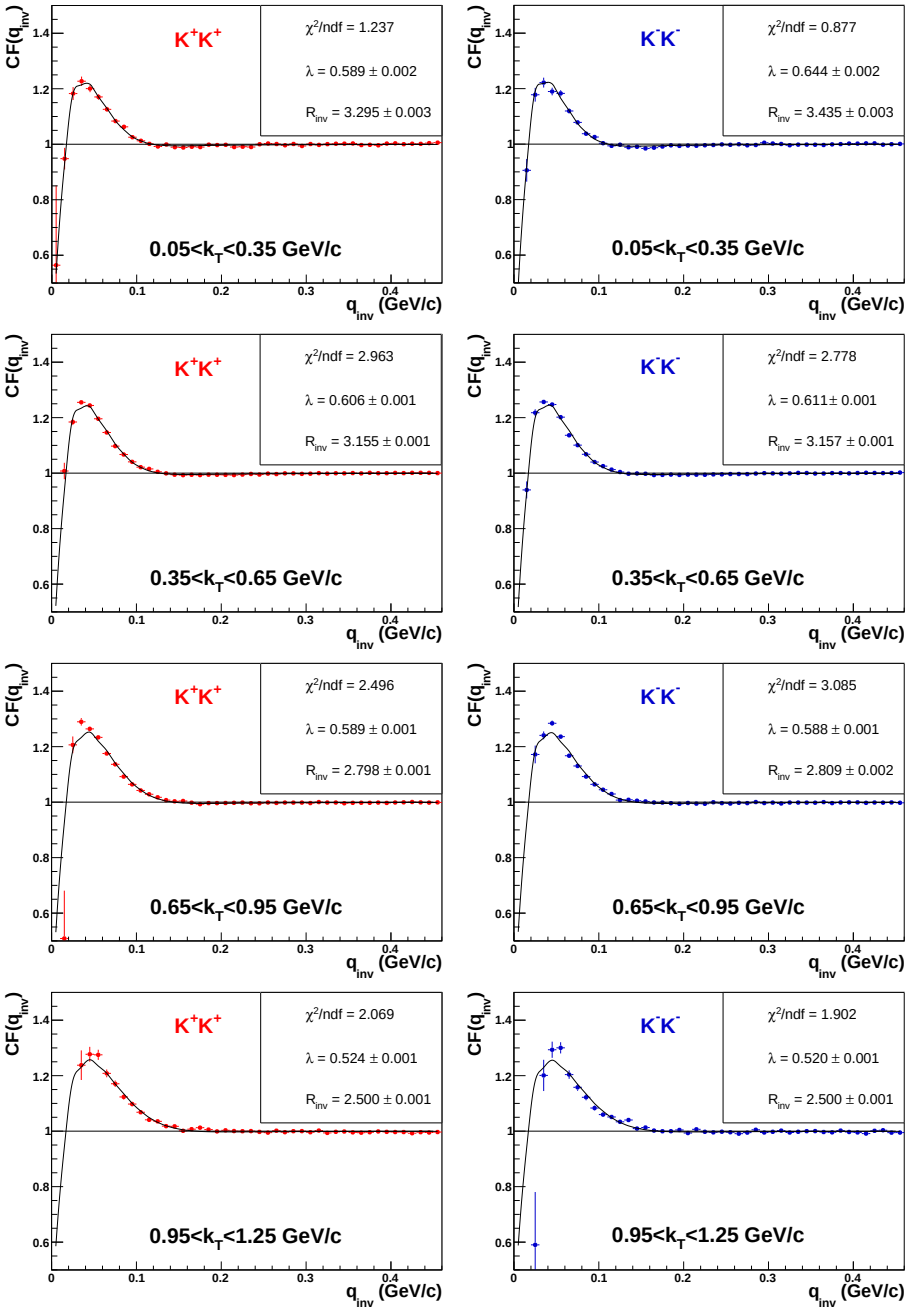

Fig. 4.3: L: Fitted K^+K^+ correlation function for different k_T bins and for centrality 30-50%. P: Fitted K^-K^- correlation function for different k_T bins and for centrality 30-50%.

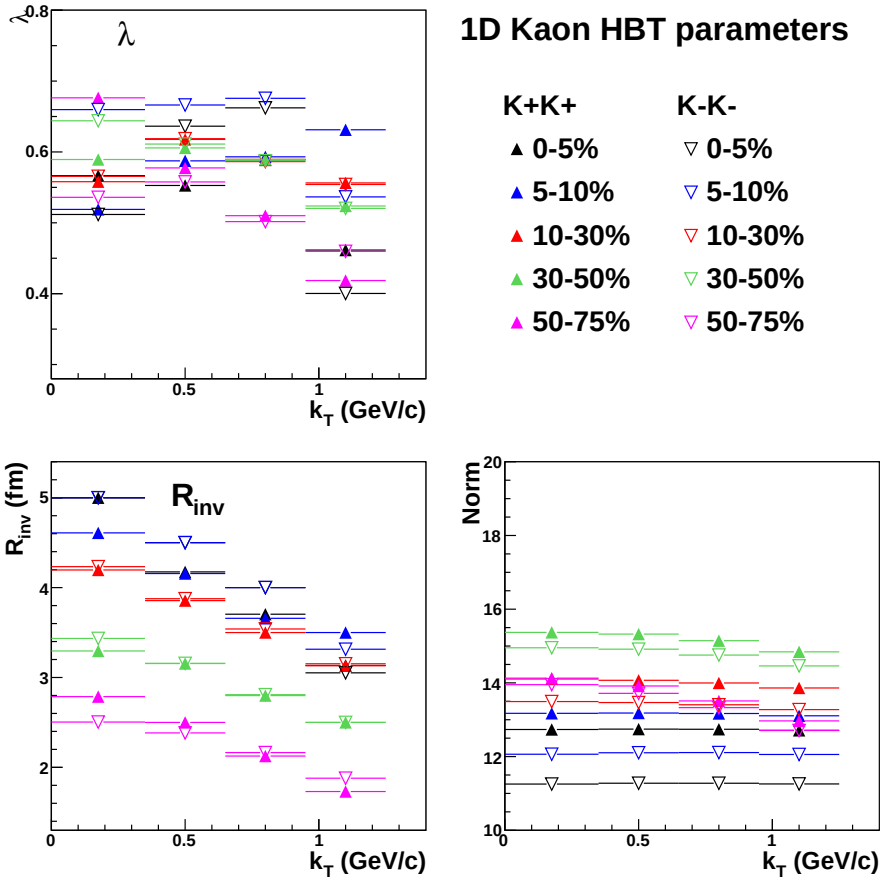

Fig. 4.4: Results from fitting like-sign correlation function. The source radii R_{inv}, λ parameter and normalization N showns as function of k_T and centrality.

4.3 Unlike-sign correlation function

Despite using so far charged kaons, the correlation function for unlike-sign pairs differs from earlier presented correlation function for like-sign pairs, but they are still sensitive to the source size. Since each kaon in pair carries opposite charge, the Coulomb interaction is now attractive. As can be seen in the Fig. 4.5, this Coulomb interaction is dominant at low relative momentum q_{inv}. In this figure, one can observe significant peak at $q_{inv} = 0.252$ GeV/c, which corresponds to strong final state interaction between unlike-sign kaon.

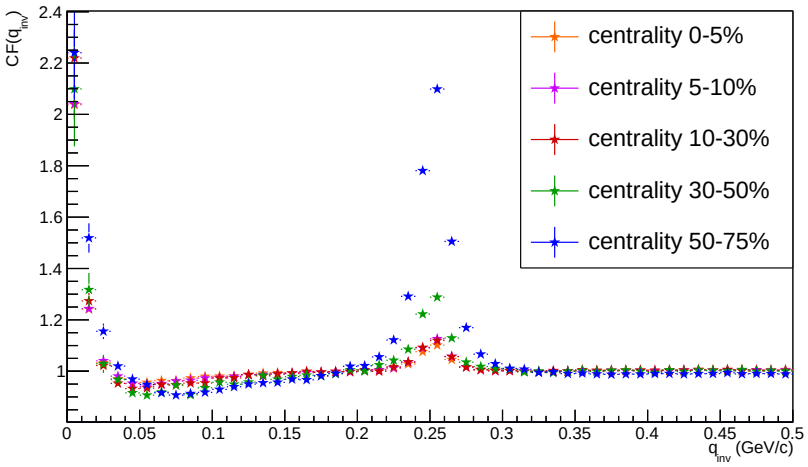

Fig. 4.5: One dimensional unlike-sign correlation function for different centralities.

As already discussed, for femtoscopy with non-identical particle, it is most suitable to used pair's rest frame, where each particle has momentum k^* and then to construct correlation function as function of k^*. This k^* is the same as the decay momentum of the system in its CMS. Therefore k^* is directly connected to the invariant mass M_{inv} of the system. Since $q_{inv} = 2k^*$, also q_{inv} is directly connected to the invariant mass. Especially in our case, relation between invariant and q_{inv} is given by formula

$$q_{inv} = \sqrt{M_{inv}^2 - 4m_K^2}. \tag{4.2}$$

Hence the peak at $q_{inv} = 0.252$ GeV/c really corresponds to $\phi(1020)$ resonance.

In this region, the centrality dependence as well as k_T dependence, which is shown in the Fig. 4.6, are observed. In both of them we can see that at low q_{inv}, where the Coulomb interaction exhibits the correlation function is not so much sensitive as in the resonance region. In addition, in the ϕ (1020)

resonance region the higher statistics is available, thus the correlation function is not statistically impaired like in Coulomb region.

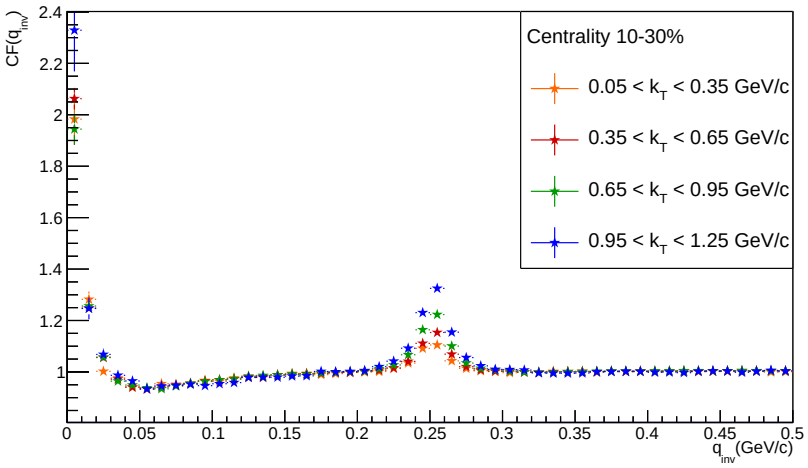

Fig. 4.6: One dimensional unlike-sign correlation function for different k_T bins.

One of the possible way how to learn something from the measured unlike-sign correlation function is to compare with one obtained from model or calculated theoretical prediction. In following two sections, we will introduce the comparison with hydrodynamics model HYDJET++ and to Lednicky model.

4.4 Comparison of unlike-sign correlation function with HYDJET++ model

Firstly, we have compared of measured correlation functions with function, which we obtained from hydrodynamics model. For our purpose, we have decided to employ HYDJET++, which was already presented in previous chapter.

HYDJET++ contains default setup of parameters for describing Au+Au collisions at $\sqrt{s_{NN}} = 200$ GeV, which are summarized in Table 4.1. With this setup were the observables like particle spectra and its ratio, v_2, source radii from $\pi - \pi$ correlation were successfully described as was introduced also in previous chapter.

Therefore we employed HYDJET++ with the same setup and we have just turn-off effect of JETs. From HYDJET++ we are able by applying the same kinematic cuts, namely cut on pseudorapidy η and momentum p on kaon sample, to obtain unlike-sign correlation function. Since HYDJET++ does not contain Coulomb interaction and strong final state interaction,only the peak in

Parameter	Value
T_{ch} (GeV)	0.165
T_{th} (GeV)	0.100
μ_B (GeV)	0.0285
μ_s (GeV)	0.007
μ_c (GeV)	0

Parameter	Value
μ_{I_3} (GeV)	-0.001
τ (fm/c)	8
$\triangle\tau$ (fm/c)	2
R (fm)	10
γ_S	1

Table 4.1: Parameters of the HYDJET++ model used for simulations

the ϕ resonance region will be presented. This peak corresponds to the thermal production of ϕ resonance.

For quantitative description, we have to do purity correction of measured raw correlation function. Since λ parameter contains all imperfections, in femtoscopy we can do purity correction via it according to formula:

$$CF^{corr} = \frac{CF^{raw} - 1}{\lambda} + 1, \tag{4.3}$$

where λ was obtained from fitting like-sign correlation function.

The comparison of the corrected experimental correlation function with function obtained from HYDJET++ is shown in the Fig. 4.7, where the correlation for one centrality is presented. It should be noted that correlation function from HYDJET++ are uncorrected.

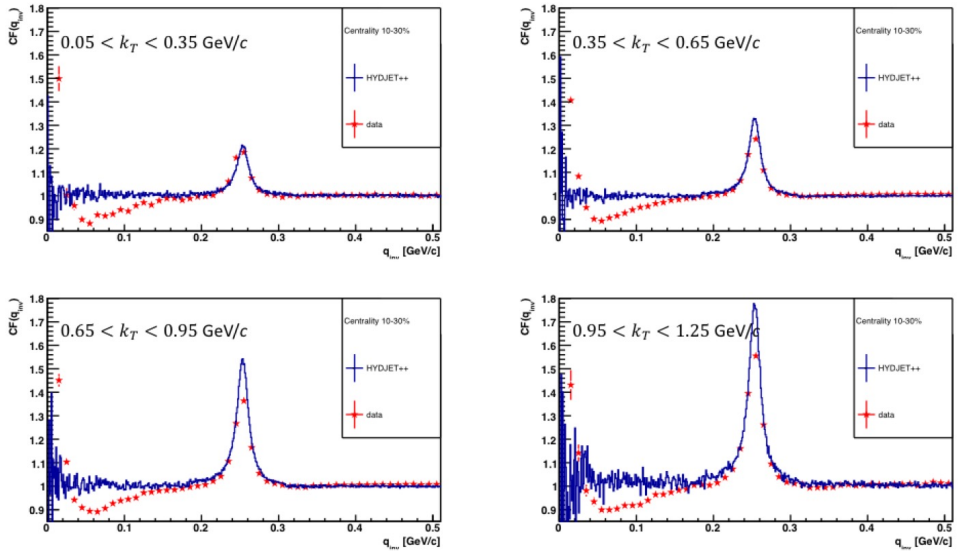

Fig. 4.7: One dimensional unlike-sign correlation function for collisions with centrality 10-30% compared with HYDJET++ simulations.

As we can see HYDJET++ produce correlation functions well especially in the ϕ resonance region for all k_T bins and for centralities.

4.5 Comparison of unlike-sign correlation function to Lednicky model

For better understanding of measured unlike-sign correlation function, we have done also theoretical calculation of them. The correlation function already presented as

$$C\left(\vec{p_1},\vec{p_2}\right) = \int d^3rS\left(r,k^*\right)\left|\psi_{1,2}\left(r,k^*\right)\right|^2, \tag{4.4}$$

contains two particle emission function $S\left(r,k^*\right)$ and wave function $\left|\psi_{1,2}\left(r,k^*\right)\right|$ describing interaction of two emitted particle.

The simplest model for emission function is the Gaussian parametrization, in which there is no correlation between the particle momenta and emission coordinates. The size of source was chosen so that to be equal to value of source radii R_{inv} obtained from fitting like-sign correlation function as shown in the Fig. 4.4.

The interaction of two kaons was calculated by Lednicky model including the treatment of the ϕ resonance due to the FSI as well as generalized smoothness approximation.

In order to compare to an experimental correlation function, the clean theoretical function is transformed to a raw one via

$$CF^{raw} = \left(CF^{corr} - 1\right)\lambda + 1. \tag{4.5}$$

Also in this case, the λ parameter is coming from fitting like-sign correlation function.

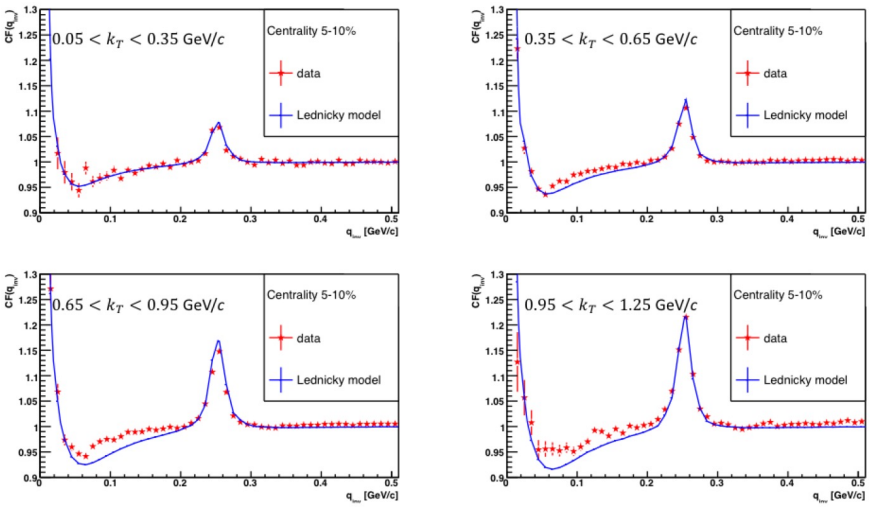

Fig. 4.8: One dimensional unlike-sign correlation function for the most central collisions compared to Lednicky model.

As we can see in the Fig. 4.8, for the most central collision Lednicky model described correlation function well at low q_{inv}, where the Coulomb and strong interaction in s-wave are presented as well as at the resonance region. Observed difference at low q_{inv} for $0.65 < k_T < 0.95$ GeV/c can be possibly ascribed to effect of residual correlation.

For case of collisions with centrality 10-30%, which are shown in the Fig. 4.9, there is still good agreement of Lednicky model with experimental constructed correlation function. However we may notice that for the higher k_T bin, Lednicky model starts to deviate from the measured correlation function in description of correlation function in the ϕ region. One of possible explanation of failure can be non-validity smoothness assumptions for pair with so high transverse momentum.

With decreasing centrality, see the Fig. 4.10, Lednicky model produces correlation function well at low q_{inv} in region where the well-known Coulomb and strong interaction are dominant. However in region of the ϕ resonance, the correlation functions are considerably underestimated.

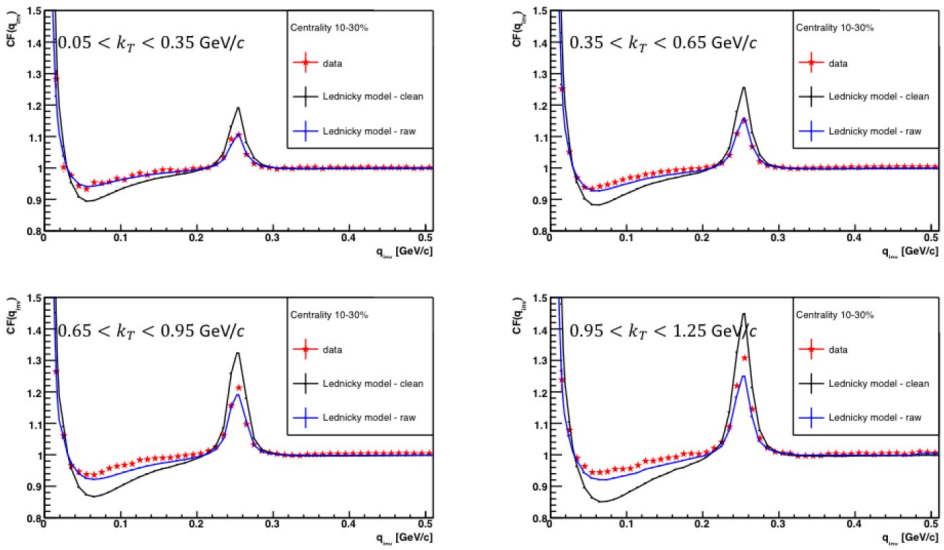

Fig. 4.9: One dimensional unlike-sign correlation function for collisions with centrality 10-30% compared to Lednicky model.

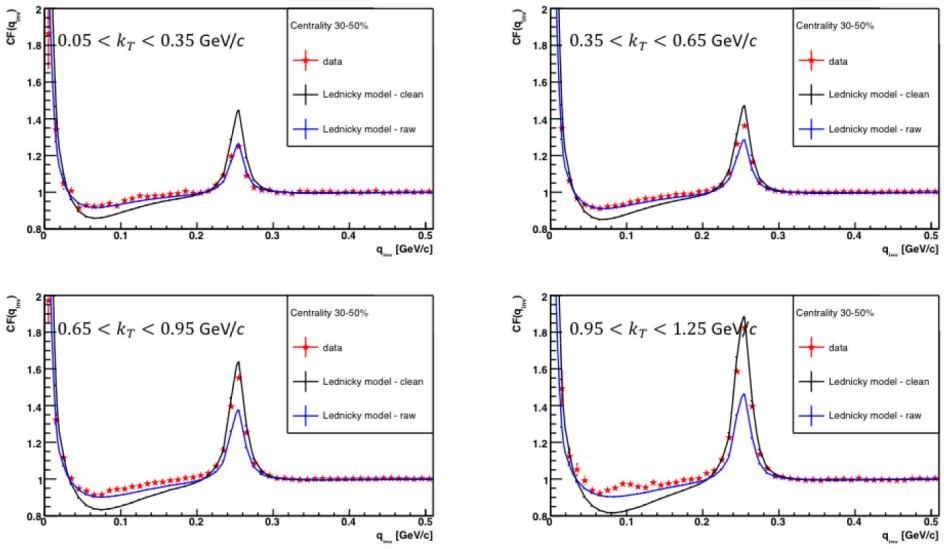

Fig. 4.10: One dimensional unlike-sign correlation function for collisions with centrality 30-50% compared to Lednicky model.

Chapter 5

Conclusions and Outlook

The main goal of this research project was to study space-time characteristics of the system created in the heavy ion collisions with unlike-sign kaon femtoscopy.

As was predicted correlations due to the strong FSI in a system where a narrow resonance is present will be sensitive, in the region of the resonance, to the source size and momentum-space correlations. The system of unlike-sign pairs is ideally suited for this measurement, since it contains narrow $\phi(1020)$ resonance. In this research project a status report of a STAR analysis of unlike-sign kaon femtoscopics correlations in Au+Au collisions at $\sqrt{s_{NN}} = 200$ GeV presented.

First, the kaon were selected from the minimum bias Au+Au collisions. Consequently, the detector effects arising from tracking imperfection were removed by the pair cut. Due to high statistics, we are able to construct one dimensional correlations for 4 k_T bins and 5 different centralities. The measured correlation function have shown significant centrality dependence as well as k_T dependence.

Finally, in order to compare of experimental correlation function to HYDJET++ simulations and with Lednicky model, the like-sign correlation function were obtained and used for extraction of kaon emission source size R_{inv} and λ parameter. The source radii R_{inv} increase with the centrality and decrease with pair transverse momentum k_T. The λ parameter was used for purity correction of unlike-sign correlation function.

HYDJET++ model reproduces the correlation functions well in the region of the resonance. In the most central collision, the Lednicky model also describes the correlation function well in the region of the resonance as well as in region of very low q_{inv}, where the Coulomb interaction and strong interaction in s-wave are presented. With decreasing centrality, the correlation function are underpredicting in region of the resonance by Lednicky model.

The analysis of unlike-sign kaon femtoscopis correlation in Au+Au collisions has not yet been finished. According to high statistics, it will be available to construct three dimensional correlation. The future work will also include detailed study of systematics uncertainties and efficiency for final comparison and extract kaon emission source size from correlation function in region of the ϕ resonance.

Bibliography

[1] Robert Hanbury; Richard Q. Twiss Brown. A test of new type of stellar interferometer on sirius. *Nature*, 178(4541):1046–1048, 1956.

[2] Gerson Goldhaber". Influence of bose-einstein statistics on the antiproton-proton annihilation process. *Physical Review*, 120(1):300–312, 1960.

[3] Michael Annan Lisa, Scott Pratt, Ron Soltz, and Urs Wiedemann. Femtoscopy in relativistic heavy ion collisions. *Ann.Rev.Nucl.Part.Sci.*, 55:357–402, 2005.

[4] R. Lednicky. Femtoscopic correlations and final state resonance formation. *Phys. Part. Nucl. Lett.*, 8:965–968, 2011.

[5] Petr Chaloupka. *Femtoscopy with multi-strange baryons at RHIC*. PhD thesis, Charles University in Prague, 2010.

[6] Mercedes Lopez Noriega. *Pion Interferometry in AuAu Collisions at a Center of Mass Energy per Nucleon of 200 GeV*. PhD thesis, The Ohio State University, 2004.

[7] Fabrice Retiere and Michael Annan Lisa. Observable implications of geometrical and dynamical aspects of freeze out in heavy ion collisions. *Phys.Rev.*, C70:044907, 2004.

[8] I.P. Lokhtin, L.V. Malinina, S.V. Petrushanko, A.M. Snigirev, I. Arsene, et al. Heavy ion event generator HYDJET++ (HYDrodynamics plus JETs). *Comput.Phys.Commun.*, 180:779–799, 2009.

[9] N. S. Amelin, R. Lednicky, I. P. Lokhtin, L. V. Malinina, A. M. Snigirev, Iu. A. Karpenko, Yu. M. Sinyukov, I. Arsene, and L. Bravina. Fast hadron freeze-out generator. Part II. Noncentral collisions. *Phys. Rev.*, C77:014903, 2008.

[10] L. Adamczyk et al. Freeze-out dynamics via charged kaon femtoscopy in sqrt(sNN) = 200 GeV central Au + Au collisions. *Phys. Rev.*, C88:034906, 02 2013.